Synthesis and Properties of Optically Active Polyaniline Carbon Nanotube Composites

Raquel Sainz,[†] William R. Small,[‡] Nigel A. Young,[‡] Cristina Vallés,[†] Ana M. Benito,[†] Wolfgang K. Maser,*[,†] and Marc in het Panhuis*[,‡,§]

Instituto de Carboquímica (CSIC), C/Miguel Luesma Castán 4, E-50018, Zaragoza, Spain, and Department of Chemistry, The University of Hull, Hull, HU6 7RX, United Kingdom

Received July 14, 2006; Revised Manuscript Received August 18, 2006

ABSTRACT: The in-situ polymerization of aniline in the presence of multiwalled carbon nanotubes and (*S*)-(+)-10-camphorsulfonic acid provides a route to optically active composite materials. Their chiroptical properties suggest that polymers and composite materials adopt similar optical properties indicative of "compact coil" in DMSO and "extended coil" in *m*-cresol. The optical activity in composite materials is preserved, although somewhat reduced to that of the pure polymer, which is attributed to the polymer phase coating nanotubes. This polymer phase is responsible for the lower electrical resistance observed for composite materials.

1. Introduction

Combining polymers with carbon nanotubes could offer the enticing prospect of materials with enhanced functionality compared to polymers.[1] Of particular interest are conducting electroactive polymers (CEP) such as the polyanilines, polypyrroles, and polythiophenes which have been recognized as suitable building blocks for intelligent materials applications as they can be engineered to recognize stimuli, are conductive, and can actuate.[2] However, the properties of CEP are lower compared to the conductivity and current carrying capacity of most metals, mechanical properties of Kevlar, and actuation stress of skeletal muscle.[1] Hence, there is room for improvement in the properties of electroactive polymers. This could be achieved by combination of these polymers with materials whose properties are superior to those of the polymers. Carbon nanotubes are an ideal candidate for such materials. Carbon nanotubes have attracted enormous attention due to their phenomenal properties.[1] For example, the mechanical and electrical properties of carbon nanotubes are several orders of magnitude higher compared to CEP such as the polyanilines (see ref 1 for a comparison). However, one of the main disadvantages of carbon nanotubes is their processability; i.e., they are not easily dispersed in most solvents due to their hydrophobic nature. This issue can be overcome by incorporating carbon nanotubes into a polymer material. This could lead to composite materials with enhanced functionality. Several preparation methods are in use for combining polymers and carbon nanotubes into composite materials. These include (but are not limited to) functionalization,[3,4] intercalation,[5] electrochemical deposition,[6] latex technology,[7] and in-situ polymerization.[8−10]

In particular, in-situ polymerization has become a standard method for producing polyaniline carbon nanotube composites, including variations such as using surfactant-stabilized multiwalled carbon nanotubes (MWNT)[11] and covalently functionalized MWNT.[12] During polymerization carbon nanotubes act as molecular templates, thereby guiding the growth of polyaniline. This facilitates interactions between polyaniline quinoids group and the nanotube surface which increase the electronic properties.[8,13]

An interesting aspect of polyaniline is its ability to become optically active through the addition of chiral dopants such as camphorsulfonic acid (CSA).[14,15] The optical activity is thought to arise from adoption of either a one-handed helical conformation[16] or a helical packing of polymer chains.[17] It is thought that chiral materials can be used as chiral films or membranes in the production of enantiomerically pure compounds.[18]

In this paper we report the synthesis of optically active polyaniline emeraldine salt multiwalled carbon nanotubes composites via in-situ polymerization of aniline in the presence of MWNT and (*S*)-(+)-10-camphorsulfonic acid. Powder materials, solutions, and supported films were characterized by a range of spectroscopic and microscopic techniques.

2. Experimental Details

Materials. Multiwalled carbon nanotubes prepared by arc-discharge (arc-MWNT) and catalytic chemical vapor deposition (CVD-MWNT). Arc-MWNT were prepared in an arc-discharge experiment by sublimation of pure graphite rods under a helium atmosphere of 66 kPa using a current of 60 A and a voltage of 25 V. Sample material was collected from the inner core of the formed cathodic deposit and consist of straight well-graphitized MWNT of micrometer lengths and 20−30 nm in diameter as well as a few graphitic nanoparticles as impurities. CVD-MWNT were prepared according to ref 19 using a Co−Mo sol−gel catalyst with a Mo/Co ratio of 30. Aniline monomer (An, distilled before use) was purchased from Scharlau, and ammonium peroxodisulfate (APS), (*S*)-(+)-10-camphorsulfonic acid (HCSA), and polyaniline emeraldine base ($M_w \sim 50\,000$) were purchased from Sigma Aldrich. All solvents—dimethyl sulfoxide (DMSO, Alfa Aesar), *n*-methyl-2-pyrrolidinone (NMP, Acros), and *m*-cresol (Riedel-de Haën)—were used as received.

In-Situ Polymerization. Composite samples were prepared by two in-situ polymerization methods of aniline in the presence of carbon nanotubes. In method 1 (similar to Zhang et al.[20]) aniline monomer was added to 110 mL of a 0.1 M HCSA solution containing arc-MWNT, while APS was dissolved in 55 mL of distilled water. Molar ratios were An:HCSA (2:1), An:APS (1:1), and 10 wt % MWNT with respect to An. Both solutions were cooled

[†] Instituto de Carboquímica (CSIC).
[‡] The University of Hull.
[§] Present address: Department of Chemistry and Intelligent Polymer Research Institute, University of Wollongong, Wollongong NSW 2522, Australia.
* To whom correspondence should be addressed: e-mail wmaser@carbon.icb.csic.es, panhuis@uow.edu.au.

10.1021/ma061587q CCC: $33.50
Published on Web 09/16/2006

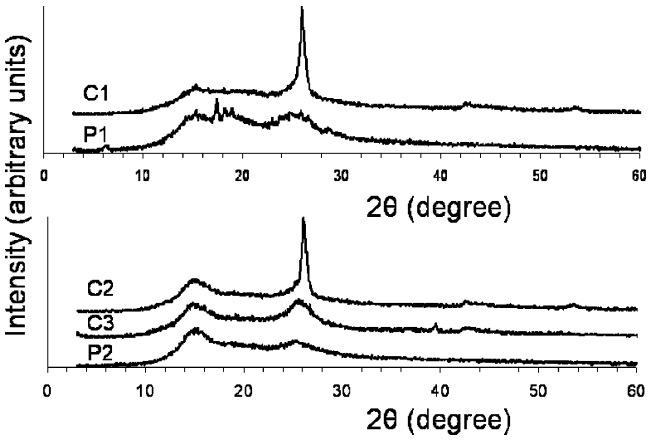

Figure 1. X-ray diffractograms of polymers (**P1**, **P2**) and composites (**C1**, **C2**, and **C3**).

(under stirring) in an ice bath (<5 °C). The oxidant solution was slowly added to the An/HCSA/arc-MWNT solution and stirred for 2 h at T < 5 °C. The resulting mixture was filtered under vacuum, washed with 390 mL of 0.1 M HCSA and distilled water, and dried at room temperature under vacuum for 24 h. Reference samples of polyaniline were synthesized under similar conditions without carbon nanotubes. These samples were labeled as **P1** (polymer) and **C1** (composite).

In method 2 (similar to Kane-Maguire et al.[21]) arc-MWNT (or CVD-MWNT) and aniline monomer were added to 100 mL of 1 M HCSA, and APS was dissolved in 5 mL of 1 M HCSA (under stirring). Molar ratios were An:HCSA (0.1:1), An:APS (4.47:1), and 10 wt % MWNT with respect to An. The oxidant solution is slowly added to the An/MWNT/HCSA solution and stirred at room temperature for $1^1/_2$ h. The resulting mixture was filtered under vacuum, washed with 400 mL of 0.1 M HCSA, and dried at room temperature under vacuum for 24 h. Reference samples of polyaniline were synthesized under similar conditions without carbon nanotubes. These samples were labeled as **P2** (polymer), **C2** (composite with arc-discharge MWNT), and **C3** (composite with CVD-MWNT).

Characterization. Powder materials were characterized by several techniques. Elemental analysis was performed in a Thermo Flash EA 1112 instrument using ~3 mg of powder materials. Scanning electron microscopy (SEM) was carried out in a JEOL JSM-6400. X-ray diffraction (XRD) was performed using a Bruker D8 ADVANCE. Infrared spectra were taken by a Bruker VERTEX 70 FTIR on pressed KBr pellets containing homogeneously dispersed powders of the corresponding materials. For thermogravimetric analysis (TGA) a Setaram TG-DTA 92 thermobalance was employed, burning 10−12 mg of powder material in air, using a flow rate of 100 mL/min and a ramp of 3 °C/min up to 1250 °C.

Table 1. Intensity (I) and Peak Position (v) for Characteristic C=C Stretching of Quinoid (Q) and Benzenoid (B) Bands

sample	I_Q	v_Q (cm^{-1})	I_B	v_B (cm^{-1})	I_Q/I_B
polymer **P1**	1.42	1574	1.42	1493	1.00
composite **C1**	2.06	1576	2.05	1491	1.03
polymer **P2**	1.91	1558	1.97	1477	0.97
composite **C2**	2.39	1558	2.42	1478	0.98
composite **C3**	2.18	1558	2.22	1478	0.98

All solutions were prepared by dissolving up to 2.5 mg of polymer or composite materials in 5 mL of solvent. Supported films were prepared by drop-casting from solution (0.5 mg/mL) onto cleaned glass slides, followed by drying at 85 °C in a vacuum oven. Thickness of supported films (2−11 μm) was determined from topographical analysis of PDMS casts of the films carried out using a scanning white light interferometer (Veeco, Wyko NT1100) as described in detail in ref 22.

Electronic absorption spectra of solutions (DMSO, NMP, and *m*-cresol) and supported films were recorded using Cary 5E UV−vis−NIR and Jasco V560 UV/vis spectrophotometers. Circular dichroism spectra were recorded using a Jasco J810 circular dichromator. All spectra were recorded 1 h after dissolving in solution as the position of the high wavelength polaron band (in solution) red shifts with time.

Transmission electron microscopy (TEM) images were obtained on a JEOL 2011 TEM. Diluted composite solutions were evaporated onto Cu 300 mesh grids. The current−voltage characteristics across supported films were determined from the constant voltage method using a Manson EP-613 power source and a Thurlby Thandar Instruments 1906 digital multimeter.

3. Results

Elemental Analysis. The extent of camphorsulfonic acid doping is calculated using elemental analysis. As HCSA does not contain any nitrogen, the percentage of polyaniline can be calculated from nitrogen analysis (see Table S1, Supporting Information). The calculated molar ratio of polyaniline tetramer unit and HCSA is 1:1 (composite **C1**, polymer **P1**) and 1:1.7 (all other samples). This suggests that polyaniline synthesized using method 1 is partially doped and almost fully doped using method 2. The carbon nanotube content in the composite samples is estimated at ~20% based on elemental analysis data.

X-ray Diffraction. The X-ray diffraction patterns of polymers **P1** and **P2** (Figure 1) showed the three characteristic peaks

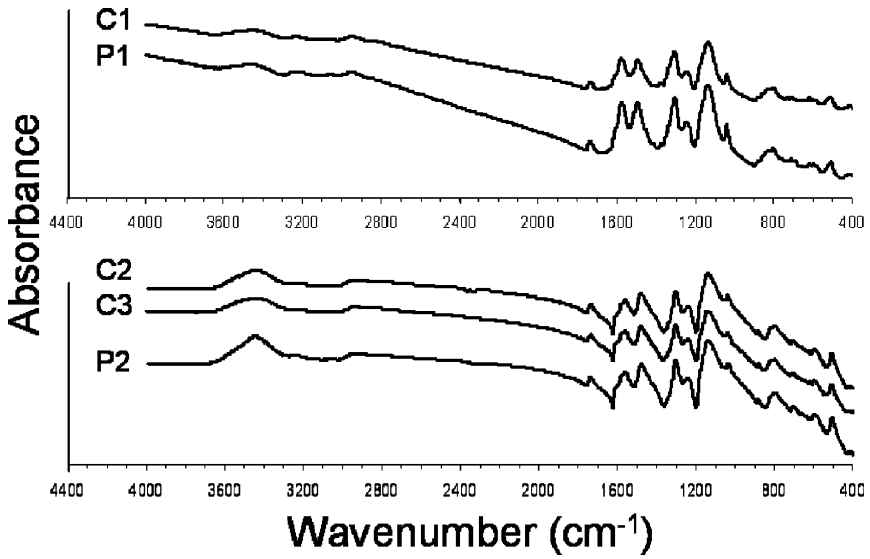

Figure 2. Fourier transform IR spectra of polymers (**P1**, **P2**) and composites **C1**, **C2**, and **C3**. Spectra are offset for clarity.

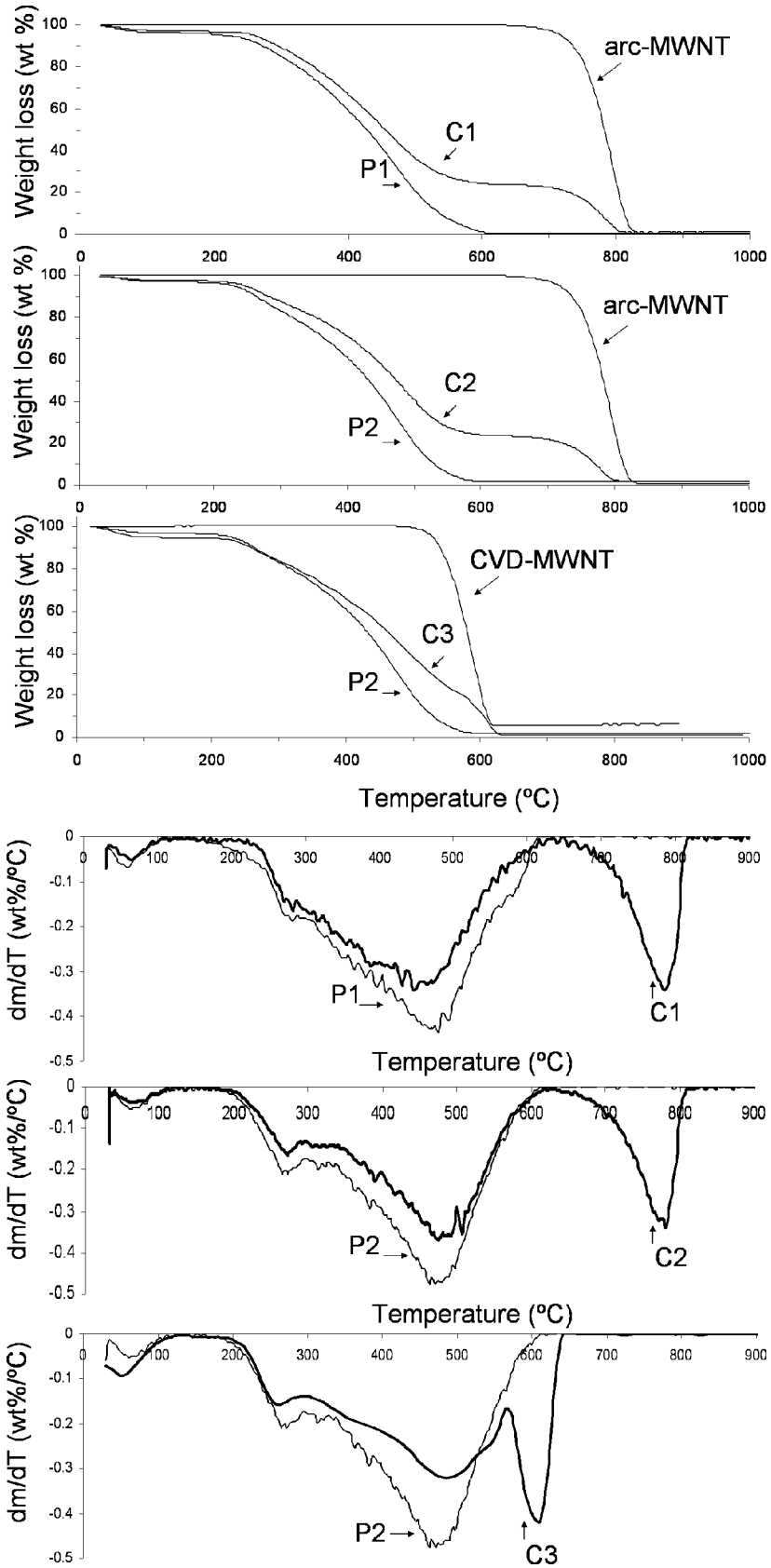

Figure 3. Thermogravimetric analysis (weight loss and derivative) of polymers (**P1**, **P2)**, composites (**C1**, **C2**, and **C3**), and carbon nanotubes (arc-MWNT, CVD-MWNT).

centered at $2\theta = 15°$, 19°, and 25° associated with polyaniline in emeraldine salt form.[23−26] The additional peaks (at $2\theta = 26°$, 42.5°, 53.5°, and 78°) observed in the patterns for composites **C1** and **C2** are typical for the presence of arc-MWNT (see Figure S1, Supporting Information), while the additional peaks (at $2\theta = 26°$, 39.6°, and 43°) observed in composite **C3** are typical for CVD-MWNT (see Figure S1).

In addition, for sample **P1** an additional peak (at $2\theta = 6.4°$) can be observed, which does not appear in any of the other samples. The presence of the peak at $2\theta = 6.4°$ has previously

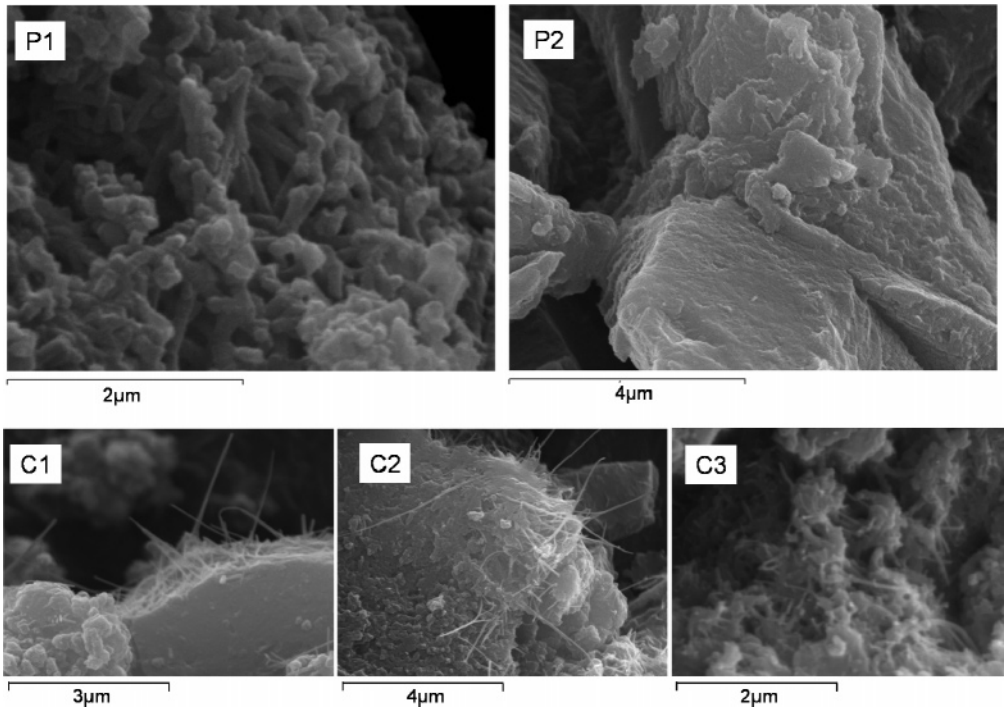

Figure 4. Scanning electron microscopy (SEM) images on powder samples of polymers (**P1**, **P2)** and composites (**C1**, **C2**, and **C3**).

been used as an indicator for polyaniline chains organized into nanofibers or lamellae.[20,27,28] This indicates that **P1** contains tubular or lamellar morphology, while **P2** and all other samples are granular. For example, tubular morphology can be explained by a mechanism based on anilinium and CSA^- micelles. Polyaniline grows inside the micelles in the form of nanofibers.[6] The absence of the tubular peak in **C1** indicates that the presence of arc-MWNT during polymerization prohibits polyaniline tubular formation. MWNT can act as nucleation points for the polymerization of polyaniline instead of growing inside the micelles.

FT-IR. The infrared spectra of polymers and composites are shown in Figure 2. The characteristic peaks of polyaniline in emeraldine salt (ES) form, for example, N−H stretching vibration (3450 cm^{-1}), C═C stretching of quinoid (Q, 1576 cm^{-1}) and benzenoid (1493 cm^{-1}), C−N stretching mode (1303 cm^{-1}), and N═Q═N (1136 cm^{-1}), were observed.[9,27,29] It is well-known that for polyaniline ES intensity of the quinoid band should be lower than that of the benzenoid band.[30] In the presence of carbon nanotubes the relative intensity of the quinoid band increases as observed for polyaniline emeraldine base (EB)[9] and ES[31] composites.

The following differences can be observed for samples prepared using methods 1 and 2 (as shown in Table 1): (i) the relative intensity of the quinoid band (with respect to benzoid band) is >1 for samples prepared using method 1, while this is <1 for samples prepared using method 2. (ii) The quinoid and benzenoid peaks have red-shifted by ∼15 cm^{-1} using method 2, indicative of a more semiquinoid form.[32] (iii) Spectra for samples prepared using method 2 have the "Fano" shape characteristic for doped polyaniline.[33] These differences are further evidence that the doping level in samples synthesized using method 1 is lower compared to samples synthesized using method 2.

Thermogravimetric Analysis. The TGA results are shown in Figures 3 and S2 (Supporting Information). The polymers (**P1**, **P2**) exhibit the three-step decomposition pattern characteristic for doped polyaniline: release of water molecules (<100 °C), dopant anion (180−280 °C), and decomposition of polyaniline chain structure (280−630 °C).[34] For composite materials an additional fourth step is observed related to the decomposition of either arc-MWNT (**C1**, **C2**) or CVD-MWNT (**C3**). The weight loss ranges for arc-MWNT and CVD-MWNT are 660−840 and 470−630 °C, respectively. The difference in oxidation temperatures is related to the degree of graphitization of the nanotubes, which is higher for arc-discharge produced MWNT.

The synthesis method and nanotubes both have an effect on the decomposition behavior of the composite samples. The difference between the synthesis methods is reflected in the higher weight loss in the second step related to the higher degree of doping for polymer **P2**. This is most clearly observed by the sharper minimum in the TGA derivative (Figure 3).

Interestingly in composite **C2** the minimum for the polymer phase (in the TGA derivative) has shifted to a higher temperature compared to that of polymer **P2**, while the minimum for the arc-MWNT has shifted to lower temperature compared to that of (pure) arc-MWNT. It is clear that this is not related to the presence of pure MWNT (see Figure S2). This difference in thermal behavior was previously attributed to the existence of a new polymer/MWNT phase.[9] A similar effect could be occurring for composite **C3**, but we cannot see this because of the overlap between decomposition of CVD-MWNT and polyaniline chain structure.

Electron Microscopy. SEM is an excellent technique for investigating the morphology of polymers and composites. Tubular (fibrular) and granular morphologies are observed for polymers **P1** and **P2**, respectively (see Figure 4). The polymer morphology depends on the reaction conditions as previously observed by Yang and Wan.[27] However, the polymer morphology is changed to granular in the presence of MWNT as shown for composite **C1**. In all composites MWNT are readily identified as the thin lines.

The wetting between polymers and carbon nanotubes in a composite can be investigated by TEM.[10] Typical TEM images

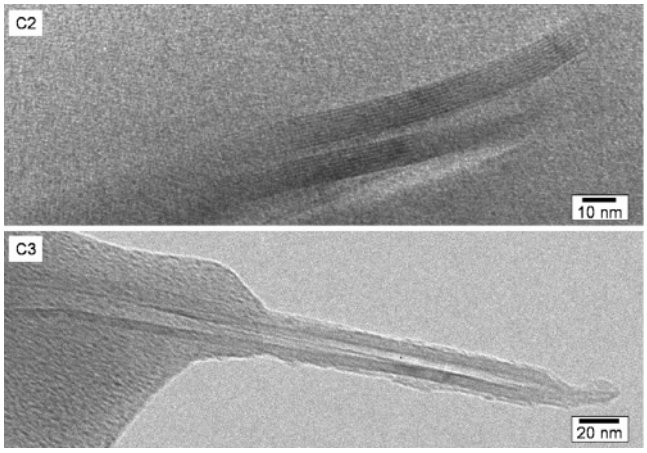

Figure 5. Transmission electron microscopy (TEM) images on evaporated solutions of composites **C2** and **C3**.

of evaporated solutions of composites **C2** and **C3** are shown in Figure 5. In general, carbon nanotubes are identifiable as thin lines with the hollow core visible within as can be seen for composite **C3**, while the image for composite **C2** shows that this particular arc-MWNT consists of nine carbon cylinders. In all images it was found that MWNT are evenly covered by polymer, indicating excellent polymer wetting of the nanotubes' surface.

Chiroptical Properties. The materials were soluble in a range of solvents (NMP, DMSO, or *m*-cresol). However, the solution spectra were dependent on the nature of the solvent and the concentration. Dispersing more than 1.5 mg in 5 mL of DMSO resulted in stable green solutions, indicative of polyaniline in emeraldine salt (ES) form. Note that no additional doping with HCSA was necessary. The UV−vis absorption spectra (at concentration 0.5 mg/mL, Figure 6) showed the three characteristic absorption bands 340, 430, and 860 nm associated with $\pi-\pi^*$, polaron$-\pi^*$, and $\pi-$polaron band transitions of polyaniline ES.[10,23] There are two distinctive polyaniline conformations: "compact coil" (tightly coiled chains) with a characteristic localized polaron band at 800 nm and "extended coil" (expanded chains) with a characteristic intense broad absorption band in the near-infrared.[10,23] The spectral features of our polymers and composites (in DMSO) are consistent with a "compact coil" formation.

Previously it has been noted that in DMSO partial deprotonation of polyaniline ES to EB occurs at dilute concentrations (0.5 mg in 5 mL of solvent).[21] The appearance of both a band at 630 nm due to EB and a localized polaron band (>750 nm) due to ES is indicative of this solvent-induced dedoping effect.[21]

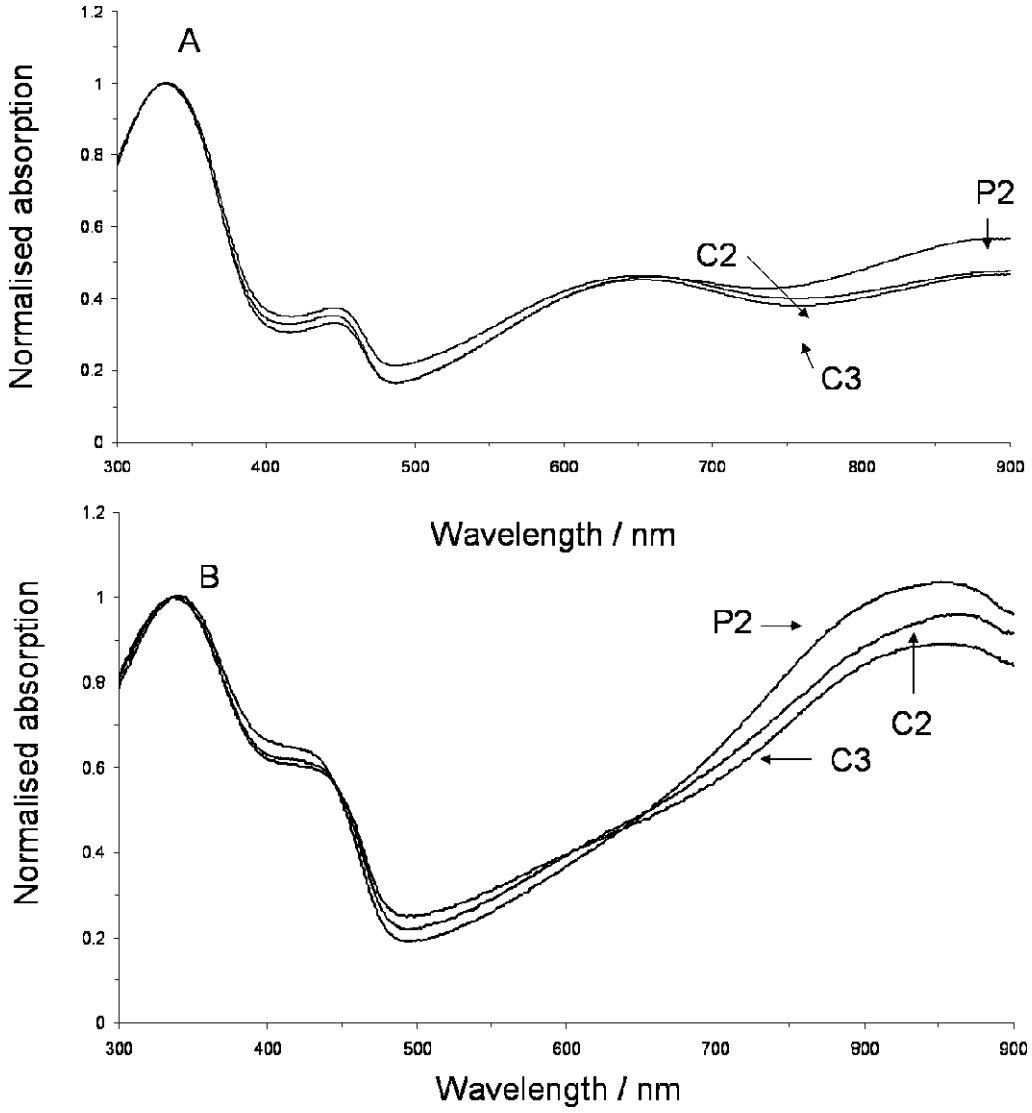

Figure 6. UV−vis absorption spectra (normalized) for polymer **P2**, composite **C2**, and composite **C3** at different sample concentrations in DMSO: (A) 0.1 mg/mL and (B) 0.5 mg/mL.

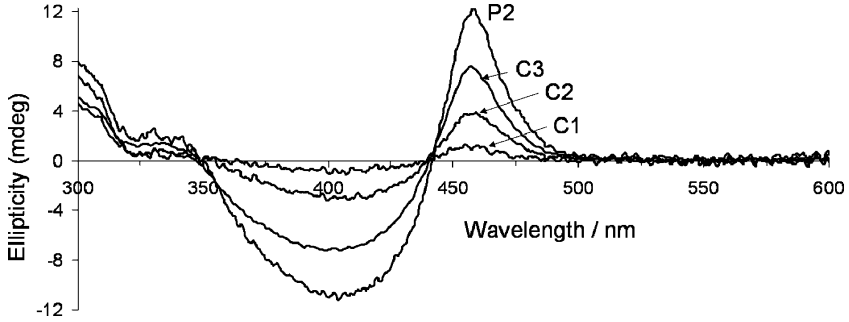

Figure 7. Circular dichroism spectra of polymer **P2** and composites **C1, C2**, and **C3** at concentration of 0.5 mg/mL in DMSO.

Table 2. Quantitative Measure (ES/EB) for Deprotonation of Polyaniline and Composite Samples Calculated Using UV−Vis Absorption of Samples at Different Concentrations in DMSO[a]

sample	ES/EB [0.1 mg/mL]	ES/EB [0.5 mg/mL]
commercial EB	0.01	2.0
polymer **P1**	0.8	1.1
composite **C1**	0.9	1.1
polymer **P2**	1.2	2.7
composite **C2**	1.1	2.3
composite **C3**	1.1	2.2

[a] ES/EB indicates ratio of UV−vis absorptions at maximum >750 and ~630 nm corresponding to ES polaron and EB charge transfer (between quinoid and benzenoid units) bands. Typical UV−vis spectra are shown in Figure 6.

Scheme 1. Strong, Loose, and Free Refer to Polymer Adsorption Levels onto Nanotube Surface

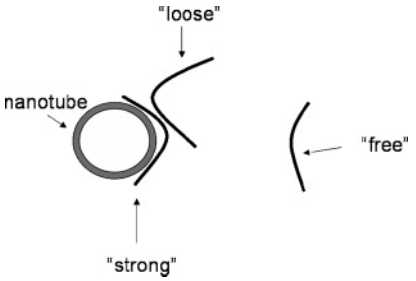

Complete deprotonation was observed at similar concentrations in NMP,[21] but not in *m*-cresol (see Figure S3, Supporting Information).

The distinctive absorption features of the two forms of polyaniline are used to provide a quantitative measure; i.e., the ratio of the absorption in these areas is then indicative of the level of deprotonation. For example, for commercial polyaniline all polymeric material is in EB form indicated by an ES/EB ratio of almost zero, i.e., complete dedoping (see Table 2, Figure S4, Supporting Information). Doping commercial EB with excess HCSA resulted in a ratio =2, indicating that most of the material is in ES form. Typical UV−vis absorption spectra illustrating the dedoping behavior at different concentrations are shown in Figures 6 and S5 (Supporting Information). Corresponding CD spectra showed no measurable optical activity. Addition of excess HCSA resulted in optical activity for samples **P2**, **C2**, and **C3**, while no optical activity could be observed for samples **P1** and **C1** (not shown).

The difference in doping levels between the two synthesis methods is reflected in the ES/EB ratios. Table 2 shows that the ES/EB ratio for synthesis method 2 is considerable higher compared to synthesis method 2 (see also Figure 6).

At higher concentrations dedoping effects are much less significant. For example, the ES/EB ratio increases to ~1.1 for samples **P1** and **C1** and ~2 for samples **P2**, **C2**, and **C3**. The corresponding CD spectra showed that all materials bar polymer **P1** exhibited optical activity (see Figure 7). Interestingly, despite equal doping levels optical activity is detected for composite **C1** but not for polymer **P1**. This could suggest that polymerization in the presence of MWNT directs polyaniline growth toward a chain conformation exhibiting optical activity.

The optical activity (estimated from 460 nm bands, at high concentration) of composite materials **C2** and **C3** is reduced compared to that of polymer **P2** by 66% and 33%, respectively. It is possible that the binding of polyaniline chains with the nanotube surface is responsible for this. Although almost every individual carbon nanotube is inherently optically active, a carbon nanotube mixture is unlikely to show any activity (see ref 1 for details). Therefore, it is reasonable to assume that the optical activity is due to free polymer and polymer loosely adsorbed onto nanotubes (see Scheme 1). Hence, if the presence of carbon nanotubes during synthesis introduces a new polymer phase (as observed by TGA), then it is possible that this polymer phase, presumably strongly interacting with the nanotubes' surface, will not contribute to the optical activity. It has been established that interactions with nanotubes can affect polymer conformation.[35] This is further supported by the larger optical activity observed in composites with CVD-MWNT compared to arc-MWNT. CVD-MWNT are less graphitised compared to arc-discharge MWNT, resulting in less efficient polymer chain stacking behavior or adsorption to nanotubes. Hence, the difference in amount of loosely and strongly adsorbed polymers onto nanotubes could be responsible for the difference in optical activity.

The UV−vis−NIR spectra for **P2**, **C2**, and **C3** in 0.5 mg/mL *m*-cresol showed an absorption peak at 440 nm and a steadily increasing so-called "free-carrier tail" indicative of polyaniline in "extended coil" conformation (see Figure 8).[23] It is well-known that *m*-cresol acts as a "secondary dopant" for the polyaniline chains leading to a conformational change from "compact coil" to "extended coil".[23] The difference in optical (see Figures 6 and 8) and electronic (see below) properties has been explained by the change from a localized polaron model (for "compact coil") to a delocalized polaron model (for "extended coil").[23] Because of interactions with *m*-cresol, polyaniline adopts a more planar conformation, resulting in an enhancement in conductivity (compared to interactions with solvents such as NMP).[36] The highest conductivity for polyaniline materials has been reported for films cast from *m*-cresol.[37]

While the UV−vis−NIR spectra of polymer **P2** and composites (**C2**, **C3**) are very similar in solution, the corresponding spectra (Figure 8) for supported films (cast from 0.5 mg/mL *m*-cresol solutions) are different. Supported films of **P2** and **C2** exhibit absorption features characteristic of both "compact coil" conformation (820 nm) and broad free carrier tail characteristic of "expanded coil" conformation (>1000 nm). The supported

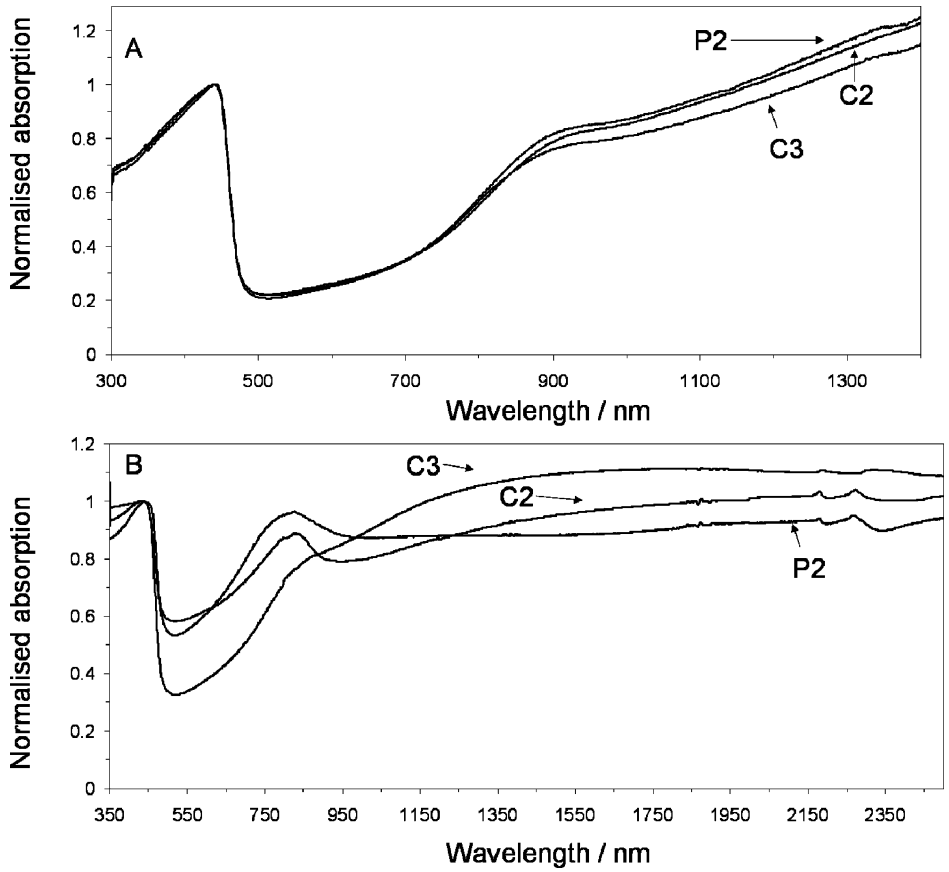

Figure 8. UV−vis−NIR absorption spectra (normalized) in *m*-cresol (A) and cast as films on glass slides (B) for polymer **P2** and composite **C2** and **C3**. Concentration 0.5 mg/mL.

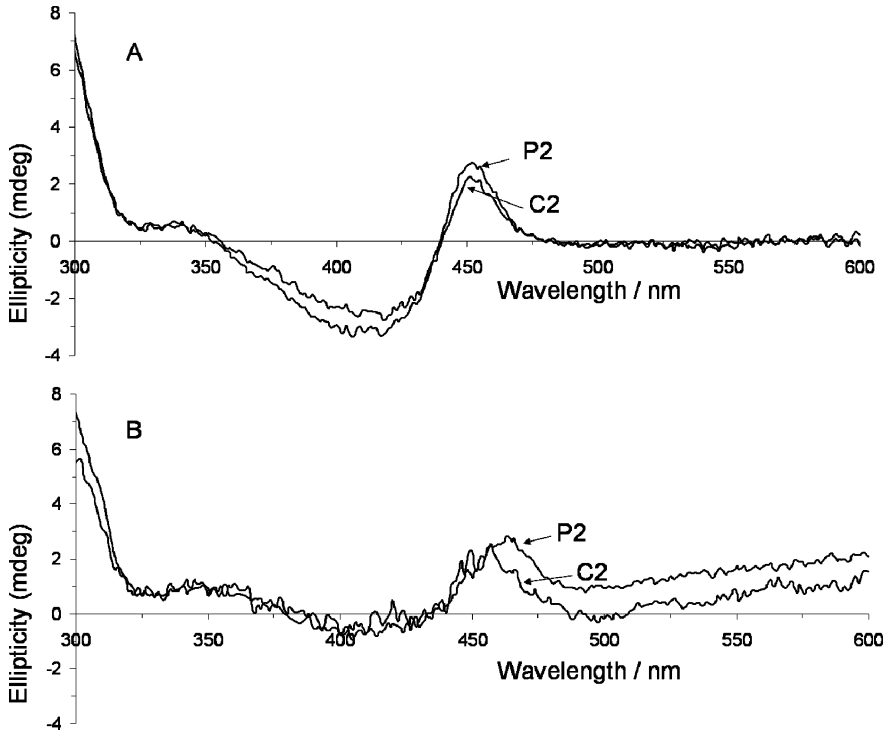

Figure 9. Circular dichroism spectra of polymer **P2** and composites **C2** (A) in *m*-cresol and (B) supported films. Concentration 0.5 mg/mL *m*-cresol.

film of **C3** is similar to that of **C2** at long wavelengths, but with a weaker absorption feature at 820 nm. The emergence of a feature indicative of "compact coil" conformation in cast films is most likely due to *m*-cresol evaporation effects. In particular, there are differences in the free carrier tails between polymer and composites, which are reflected in the electrical resistance of the supported films (as discussed below).

The optical activity of **P2** and **C2** in *m*-cresol solutions (Figure 9) is less intense compared to solutions in DMSO, which could be due to interactions between *m*-cresol, HCSA, and

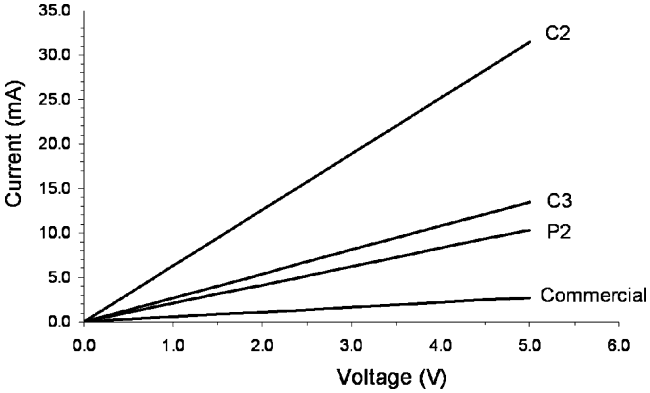

Figure 10. Current−voltage characteristics in air of **P2**, **C2**, and **C3** and commercial polyaniline (doped with HCSA). Measurements carried out on supported films cast from 0.5 mg/mL *m*-cresol solutions.

Table 3. Resistances for Supported Films of P2, C2, C3, and Commercial Polyaniline (Doped with HCSA) Evaluated from Current−Voltage Characteristics (See Figure 9)

film	resistance (Ω)[a]
P2	512 ± 14
C2	157 ± 2
C3	378 ± 9
commercial polyaniline	1836 ± 23

[a] Errors were evaluated from three independent measurement sets.

polyaniline chains. The optical activity is retained in supported films (see Figure 9).

Electrical Properties. It is well-known that the conductivity for films cast from *m*-cresol is several orders of magnitude higher compared to films cast from solvents such as DMSO or NMP.[23] The current−voltage (*I*−*V*) characteristics of supported films cast from 0.5 mg/mL *m*-cresol were investigated. For all films linear characteristics were observed, indicating ohmic behavior. The calculated resistance for supported films cast from polymer **P1** and composite **C1** is ∼60 MΩ. High resistances can be expected for polyaniline with low doping level, similar to nonconducting polyaniline. However, for composite **C1** a significantly lower resistance was expected due to the presence of arc-MWNT. A material consisting of nonconducting polymer and conducting nanotubes exhibits a significant increase in conductivity for concentrations above the percolation threshold or the concentration needed to form electrical pathways through the sample. The absence of a decrease in resistance for composite **C1** suggests either a nanotube concentration below the percolation threshold or polyaniline coating of the nanotubes causing a tunneling barrier between nanotubes. The latter has been suggested for in-situ polymerized (nonconducting) polyaniline EB in the presence of arc-MWNT.[9]

The *I*−*V* characteristics for supported films of polymer **P2** and composites **C2** and **C3** are shown in Figure 10. HCSA doped commercial polyaniline results are shown for comparison. Composites **C2** and **C3** show a significantly lower resistance compared to polymer **P2** (see Table 3). The decrease in resistance (increase in conduction) for composite materials suggests conduction through either a percolated network of MWNT or a polyaniline phase with lower resistance compared to **P2**. The difference in "free-carrier" absorption features between composite (**C2**, **C3**) and polymer **P2** (Figure 8) and detection of a new phase with TGA (Figure 3) provide evidence in support of this suggestion. This point is further strengthened by the absence of a decreased resistance for composite **C1** pointing toward a (nanotube) coating of insufficiently doped polyaniline acting as a tunneling barrier between the MWNT. As the doping levels for polyaniline in **C2** and **C3** are much higher, the polyaniline coating (of MWNT) does not act as a tunneling barrier. Therefore, it is more likely that interactions between polyaniline coating and underlying MWNT could be responsible for the observed decrease in resistance.

4. Conclusions

The synthesis of optically active polyaniline carbon nanotube composite materials has been achieved via in-situ polymerization of polyaniline in the presence of MWNT. Optical activity in composite materials is preserved although somewhat reduced compared to that of pure polymer. It is suggested that this can be attributed to the polymer phase coating nanotubes, which does not contribute to the optical activity. Polymers and composites exhibited similar optical properties indicative of "compact coil" conformation in DMSO and "extended coil" conformation in *m*-cresol. However, supported films cast from *m*-cresol showed differences in the free carrier tails between polymer and composite samples. The corresponding differences in film resistances are attributed to the polyaniline coating of nanotubes, resulting in a decreased resistance in composite samples.

Acknowledgment. This work is funded by a Royal Society International Joint project (U.K. and Spain), EPSRC and the Hull Clinical Biosciences Institute. The Group of the Instituto de Carboquímica gratefully acknowledges financial support from the Regional Government of Aragon (Diputación General de Aragón, DGA) under strategic research project PIP021/2005. Mrs. J. Halder of the University of Hull Microscopy Facility is thanked for electron microscopy images. We thank the Technology Facility of the Biology Department at the University of York for use of the CD spectropolarimeter, Dr. A. Leech for assistance with CD measurements, and Dr. C. D. Walton for assistance with thickness measurements.

Supporting Information Available: X-ray diffractograms, thermogravimetric analysis, photographs, and UV−vis spectra. This material is available free of charge via the Internet at http://pubs.acs.org.

References and Notes

(1) in het Panhuis, M. *J. Mater. Chem.* **2006**, *16*, 3598.
(2) Wallace, G. G.; Spinks, G. M.; Kane-Maguire, L. A. P.; Teasdale, P. R. *Conductive Electroactive Polymers: Intelligent Materials Systems*; CRC Press: Boca Raton, FL, 2003.
(3) McCarthy, B.; Coleman, J. N.; Czerw, R.; Dalton, A. B.; in het Panhuis, M.; Maiti, A.; Drury, A.; Bernier, P.; Nagy, J. B.; Byrne, H. J.; Carroll, D. J.; Blau, W. J. *J. Phys. Chem. B* **2002**, *106*, 2210.
(4) Qu, L.; Veca, L. M.; Lin, Y.; Kitaygorodskiy, A.; Chen, B.; McCall, A. M.; Connell, J. W.; Sun, Y. P. *Macromolecules* **2005**, *38*, 10328.
(5) Frizzell, C. J.; in het Panhuis, M.; Coutinho, D. H.; Balkus, K. J., Jr.; Minett, A. I.; Blau, W. J.; Coleman, J. N. *Phys. Rev. B* **2005**, *72*, 245420.
(6) Hughes, M.; Chen, G. Z.; Schaffer, M. S. P.; Fray, D. J.; Windle, A. H. *Chem. Mater.* **2002**, *14*, 1610.
(7) Grossiord, N.; Loos, J.; Koning, C. E. *J. Mater. Chem.* **2005**, *15*, 2349.
(8) Cochet, M.; Maser, W. K.; Benito, A. M.; Callejas, M. A.; Martinez, M. T.; Benoit, J. M.; Schreiber, J.; Chauvet, O. *Chem. Commun.* **2001**, 1850.
(9) Sainz, R.; Benito, A. M.; Martinez, M. T.; Galindo, J. F.; Sotres, J.; Baro, A. M.; Corraze, B.; Chauvet, O.; Maser, W. K. *Adv. Mater.* **2005**, *17*, 278.
(10) in het Panhuis, M.; Sainz, R.; Innis, P. C.; Kane-Maguire, L. A. P.; Benito, A. M.; Martínez, M. T.; Moulton, S. E.; Wallace, G. G.; Maser, W. K. *J. Phys. Chem. B* **2005**, *109*, 22725.
(11) Zhang, X.; Zhang, J.; Wang, R.; Liu, Z. *Carbon* **2004**, *42*, 1455.
(12) Wu, T. M.; Lin, Y. W.; Liao, C. S. *Carbon* **2005**, *43*, 734.
(13) Zengin, H.; Zhou, W.; Jin, J.; Czerw, R.; Smith, D. W.; Echegoyen, L.; Carroll, D. L.; Foulger, S. H.; Ballato, J. *Adv. Mater.* **2002**, *14*, 1480.

(14) Majidi, M. R.; Kane-Maguire, L. A. P.; Wallace, G. G. *Polymer* **1994**, *35*, 3113.
(15) Pornputtkul, Y.; Kane-Maquire, L. A. P.; Innis, P. C.; Wallace, G. G. *Chem. Commun.* **2005**, 4539.
(16) Ashraf, S. A.; Kane-Maguire, L. A. P.; Majidi, M. R.; Pyne, S. G.; Wallace, G. G. *Polymer* **1997**, *38*, 2627.
(17) Langeveld-Voss, B. M. W.; Janssen, R. A. J.; Meijer, E. W. *J. Mol. Struct.* **2000**, *521*, 285.
(18) Zhang, J.; Albelda, M. T.; Liu, Y.; Canary, J. W. *Chirality* **2005**, *17*, 404.
(19) Pérez-Mendoza, M.; Vallés, C.; Maser, W. K.; Martínez, M. T.; Benito, A. M. *Nanotechnology* **2005**, *16*, S224.
(20) Zhang, L.; Wan, M. *Thin Solid Films* **2005**, *477*, 24.
(21) Kane-Maguire, L. A. P.; MacDiarmid, A. G.; Norris, I. D.; Wallace, G. G.; Zheng, W. *Synth. Met.* **1999**, *106*, 171.
(22) Small, W. R.; Walton, C. D.; Loos, J.; in het Panhuis, M. *J. Phys. Chem. B* **2006**, *110*, 13029.
(23) Xia, Y.; Wiesinger, J. M.; MacDiarmid, A. G.; Epstein, A. J. *Chem. Mater.* **1995**, *7*, 443.
(24) Yan, H.; Ohta, T.; Toshima, N. *Macromol. Mater. Eng.* **2001**, *286*, 139.
(25) Djurado, D.; Nicolau, Y. F.; Dalsegg, I.; Samuelsen, E. J. *Synth. Met.* **1997**, *84*, 121.
(26) Li, W.; Wan, M. *Synth. Met.* **1998**, *92*, 121.
(27) Yang, Y.; Wan, M. *J. Mater. Chem.* **2002**, *12*, 897.
(28) Jana, T.; Chatterjee, J.; Nandi, A. K. *Langmuir* **2002**, *18*, 5720.
(29) Huang, J. E.; Li, X. H.; Xu, J. C.; Li, H. L. *Carbon* **2003**, *41*, 2731.
(30) Quillard, S.; Louarn, G.; Lefrant, S.; MacDiarmid, A. G. *Phys. Rev. B* **1994**, *50*, 12496.
(31) Zengin, H.; Zhou, W.; Jin, J.; Czerw, R.; Smith, D. W.; Echegoyen, L.; Carroll, D. L.; Foulger, S. H.; Ballato, J. *Adv. Mater.* **2002**, *14*, 1480.
(32) Harada, I.; Furukawa, Y.; Ueda, F. *Synth. Met.* **1989**, *29*, E303.
(33) Tigelaar, D. M.; Lee, W.; Bates, K. A.; Saprigin, A.; Prigodin, V. N.; Cao, X.; Nafie, L. A.; Platz, M. S.; Epstein, A. J. *Chem. Mater.* **2002**, *14*, 1430.
(34) Kulkarni, M. V.; Viswanath, A. K. *J. Macromol. Sci., Pure Appl. Chem.* **2004**, *41*, 1173.
(35) in het Panhuis, M.; Maiti, A.; Dalton, A. B.; van den Noort, A.; Coleman, J. N.; McCarthy, B.; Blau, W. J. *J. Phys. Chem. B* **2003**, *107*, 478.
(36) Ikkala, O. T.; Pietila, L. O.; Ahjopalo, L.; Osterholm, H.; Passiniemi, P. J. *J. Chem. Phys.* **1995**, *103*, 9855.
(37) Lee, K.; Cho, S.; Park, S. H.; Heeger, A. J.; Lee, C. W.; Lee, S. H. *Nature (London)* **2006**, *441*, 65.

MA061587Q